IET Electric Power Applications

Research Article

IET Journals
The Institution of Engineering and Technology

Robust predictive current control for IPMSM without rotor flux information based on a discrete-time disturbance observer

ISSN 1751-8660
Received on 15th March 2019
Revised 17th July 2019
Accepted on 29th August 2019
E-First on 12th November 2019
doi: 10.1049/iet-epa.2019.0252
www.ietdl.org

Shin-Won Kang[1], Jae-Hwan Soh[1], Rae-Young Kim[1], Kui-Jun Lee[2], Sang-Il Kim[3] ✉

[1]*Department of Electrical and Biomedical Engineering, Hanyang University, Seoul, Republic of Korea*
[2]*Department of Electrical Engineering, Korea National University of Transportation, Chungju-si, Chungcheongbuk-do, Republic of Korea*
[3]*Department of Electrical Engineering, Daelim University College, Anyang-si, Gyeonggi-do, Republic of Korea*
✉ *E-mail: sikim@daelim.ac.kr*

Abstract: This study proposes a novel robust predictive current control that is based on a discrete-time disturbance observer for an interior permanent magnet synchronous motor (IPMSM), does not require rotor flux information. To confirm the effects of the current control response on a parameter mismatch, the parameter sensitivity for the current prediction of a conventional deadbeat predictive current control (DPCC) is analysed. With the proposed method, disturbances owing to a parameter mismatch, rotor flux term, and unmodelled dynamics are estimated using a Luenberger observer in the discrete-time domain. The estimated disturbances are compensated with the predicted reference voltage model considering a digital delay. The stability of the proposed disturbance observer owing to a parameter mismatch of the stator resistance and *d*–*q* inductance is also analysed. The proposed method is robust against the stator resistance and an inductance variation, and an accurate predicted current control can be obtained without an offline or online estimation of the rotor flux. Compared with the conventional DPCC, the proposed method can eliminate a steady-state current and transient state error caused by disturbances of the system. Experimental results are presented to verify the proposed control scheme even with mismatched parameters of the IPMSM.

1 Introduction

Permanent magnet synchronous motor (PMSM) is widely used in various industrial fields, such as industrial robots and electric vehicles, owing to its high efficiency, high output density, and excellent control performance. Therefore these applications require a fast-electrical torque response and a fast current control loop. Methods for current control include hysteresis control [1, 2], proportional-integral control [3], direct torque control [3, 4] and predictive control [5, 6]. Predictive control is generally classified into finite-control-set model predictive control (FCS-MPC) [7–11] and deadbeat predictive current control (DPCC) [12–14]. The FCS-MPC does not require a modulator, and a discrete voltage vector that minimises the cost function is chosen as the optimal vector. The FCS-MPC has a fast-dynamic response because it does not have an internal current loop and is easy to apply in non-linear systems. However, FCS-MPC generally has certain drawbacks such as a high computational burden, large current ripple, and variable switching frequency. Meanwhile, DPCC uses the system model to calculate the reference voltage vector for every sampling period and allows the inverter output current to reach the reference current value after one sampling period. DPCC uses pulse width modulation to ensure a constant switching frequency and has the advantages of a fast dynamic and low current ripple. Therefore, DPCC is used in various applications such as three-phase inverter control [13, 14] and a motor drive [12].

Although DPCC can achieve fast current response, the strong dependence problem of the system model still needs to be solved. With DPCC, the current prediction and reference voltage model of the next period are obtained using a discrete model of the motor. Therefore, the control performance depends on the parameters of the motor. Unfortunately, these parameters differ from the actual values owing to measurement errors, or the values vary depending on the motor drive conditions. Thus, motor parameter mismatches and uncertainties can cause prediction errors, and the system can become unstable.

In an interior permanent magnet synchronous motor (IPMSM), the rotor flux is equal to the permanent magnet flux linkage. A mismatch of the rotor flux has a significant influence on medium and high speeds because the back electromotive force (EMF) is proportional to the rotor flux. If the rotor flux is not correct, a constant current error occurs in steady-state, and overcurrent or undercurrent occurs in transient state. In general, because the rotor flux is difficult to measure directly, it is calculated by measuring the EMF offline by driving a load motor. However, if the ambient temperature increases or the operating condition of the motor changes owing to the large current, the rotor flux will be reduced, resulting in errors in the EMF and an adverse effect of the current control. The accuracy of the inductance, as well as the rotor flux, is also important. In general, the inductance can change dramatically owing to magnetic saturation depending on the load conditions. An inductance mismatch causes a current prediction error and oscillation, which deteriorates the current control [15, 16]. The accuracy of motor parameters such as rotor flux, inductance, and stator resistance is important in predictive current control and the system may be unstable due to the system model errors in parameters or various disturbances. Therefore, it is necessary for a method to obtain robustness against motor parameter variation.

Several robust predictive controls have been proposed to overcome this parameter sensitivity [15–23]. First, a method using the error value of the model was developed. In [18], a method to reduce the torque ripple under a parameter mismatch by adding the latest prediction error to the prediction current is proposed. Although this method is easy to implement, it is susceptible to current measurement errors and is limited to FCS-MPC. In [19], a method compensating for a parameter disturbance by a time delay control approach of the voltage equation is proposed. Although this method is also easy to implement, because of the low-pass filter, the phase delay of the calculated disturbance degrades the compensation characteristics and limits the range of robustness. Another method is an online parameter identification technique. In [20], a method overcoming a model mismatch and parameter uncertainty by estimating the input inductance and resistance of the AC–DC active front ends online is presented. In [21], an online multiparameter estimation method using a recursive least squares estimator in FCS-MPC of an IPMSM is proposed. In [22], a

position-offset based parameter estimation is used to estimate the rotor flux, along with some other mechanical parameters. Although these methods can accurately estimate the parameters in the real time, their implementation is complicated, and an offline rotor flux estimation must first be conducted, and it is difficult to obtain robustness against uncertain disturbances. Finally, a disturbance observer (DOB)-based control method has been developed. This is a good solution to system disturbances that include parameter uncertainties. Luenberger observer, a type of DOB, is used to correct the deviations between an actual system and the model used for control, and is applied in many industrial fields such as electric motors [16] and grid-connected inverter systems [15, 17, 23]. Huerta *et al*. in [23], a deadbeat control law combined with a Luenberger observer is proposed to estimate the future value of the grid currents. This offers robustness against filter and grid-impedance uncertainties. Lee *et al*. in [15], proposed a robust predictive current controller based on a Luenberger observer to estimate the parameter uncertainty and grid angle in a three-phase grid-connected inverter system. Wang *et al*. in [16], described a discrete Luenberger observer designed to estimate the future values of the stator current and parameter disturbances in the induction machine drives.

In this paper, a novel robust predictive current control (RPCC) with a discrete-time DOB that estimates the disturbance of the parameter variation online for an IPMSM drive is proposed. The contributions of the proposed observer are as follows: (i) sensitivity from uncertainty of the resistance and inductance is overcome and (ii) predictive control is possible regardless of the rotor flux information. This method is robust to the stator resistance and inductance parameters and does not require a pre-estimation or online estimation technique for the rotor flux information.

This paper is organised as follows. Section 2 describes a conventional DPCC and an analysis of the error of the predicted current according to the parameter variations. Section 3 describes the discrete-time domain of RPCC with the proposed DOB and includes a stability analysis. Section 4 verifies the effectiveness of the proposed method based on the experimental results. Finally, the conclusions are summarised in Section 5.

2 Conventional DPCC and parameter sensitivity analysis

This section briefly introduces the voltage equation of the IPMSM and the conventional DPCC method, and analyses the sensitivity to a parameter mismatch of the conventional DPCC method.

2.1 Machine equation of IPMSM

In the rotating reference frame, the voltage equation of an IPMSM can be expressed as (1) [24]

$$\begin{cases} v_d = R_s i_d + L_d \dfrac{\mathrm{d}i_d}{\mathrm{d}t} - L_q \omega_r i_q \\ v_q = R_s i_q + L_q \dfrac{\mathrm{d}i_q}{\mathrm{d}t} + L_d \omega_r i_d + \lambda_m \omega_r \end{cases} \tag{1}$$

where R_s is the stator resistance, λ_m is the permanent magnet flux linkage, ω_r is the electric angular speed, L_d and L_q are the d–q-axis inductances, i_d and i_q are the d–q-axis stator currents, and v_d and v_q are the d–q-axis stator voltages.

Expressing i_d and i_q as state variables, (1) can be rewritten as follows:

$$\begin{aligned} \begin{bmatrix} \dfrac{\mathrm{d}i_d}{\mathrm{d}t} \\ \dfrac{\mathrm{d}i_q}{\mathrm{d}t} \end{bmatrix} &= \begin{bmatrix} -\dfrac{R_s}{L_d} & \dfrac{L_q}{L_d}\omega_r \\ -\dfrac{L_d}{L_q}\omega_r & -\dfrac{R_s}{L_q} \end{bmatrix} \begin{bmatrix} i_d \\ i_q \end{bmatrix} \\ &+ \begin{bmatrix} \dfrac{1}{L_d} & 0 \\ 0 & \dfrac{1}{L_q} \end{bmatrix} \begin{bmatrix} v_d \\ v_q \end{bmatrix} + \begin{bmatrix} 0 \\ -\dfrac{\lambda_m}{L_q}\omega_r \end{bmatrix}. \end{aligned} \tag{2}$$

If the sampling period T_s is sufficiently small, (2) can be expressed as a discrete-time model in (3) by applying the Euler approximation method [25]. Here, matrices $\boldsymbol{A}$, $\boldsymbol{B}$, and $\boldsymbol{D}$ are given by (4).

$$\begin{bmatrix} i_d(k+1) \\ i_q(k+1) \end{bmatrix} = \boldsymbol{A}(k) \begin{bmatrix} i_d(k) \\ i_q(k) \end{bmatrix} + \boldsymbol{B} \begin{bmatrix} v_d(k) \\ v_q(k) \end{bmatrix} + \boldsymbol{D}(k) \tag{3}$$

$$\begin{aligned} \boldsymbol{A}(k) &= \begin{bmatrix} 1 - \dfrac{T_s R_s}{L_d} & \dfrac{L_q}{L_d} T_s \omega_r(k) \\ -\dfrac{L_d}{L_q} T_s \omega_r(k) & 1 - \dfrac{T_s R_s}{L_q} \end{bmatrix} \\ \boldsymbol{B} &= \begin{bmatrix} \dfrac{T_s}{L_d} & 0 \\ 0 & \dfrac{T_s}{L_q} \end{bmatrix} \\ \boldsymbol{D}(k) &= \begin{bmatrix} 0 \\ -\dfrac{T_s \lambda_m}{L_q} \omega_r(k) \end{bmatrix} \end{aligned} \tag{4}$$

where $i_d(k)$ and $i_q(k)$ are the d–q-axis (k)th stator currents, $i_d(k+1)$ and $i_q(k+1)$ are the d–q-axis ($k+1$)th predicted stator currents, $v_d(k)$ and $v_q(k)$ are the d–q-axis (k)th output voltages, and $\omega_r(k)$ is the (k)th rotor speed.

2.2 Conventional DPCC

According to the deadbeat control principle, because the inverter output current reaches the reference current value after one sampling period, it can be expressed as (5), assuming that the current reference is constant $\left(i_{dq}^{\mathrm{ref}}(k) = i_{dq}^{\mathrm{ref}}(k+1)\right)$ [12].

$$\begin{cases} i_d(k+1) = i_d^{\mathrm{ref}}(k) \\ i_q(k+1) = i_q^{\mathrm{ref}}(k) \end{cases} \tag{5}$$

where $i_d^{\mathrm{ref}}(k)$ and $i_q^{\mathrm{ref}}(k)$ are the d–q-axis reference stator currents.

Using the discrete-time model of (3) and (5), the d–q-axis of the (k)th reference stator voltages $v_d^{\mathrm{ref}}(k)$ and $v_q^{\mathrm{ref}}(k)$ are given by

$$\begin{bmatrix} v_d^{\mathrm{ref}}(k) \\ v_q^{\mathrm{ref}}(k) \end{bmatrix} = \boldsymbol{B}^{-1} \left\{ \begin{bmatrix} i_d^{\mathrm{ref}}(k) \\ i_q^{\mathrm{ref}}(k) \end{bmatrix} - \boldsymbol{A}(k) \begin{bmatrix} i_d(k) \\ i_q(k) \end{bmatrix} - \boldsymbol{D}(k) \right\}. \tag{6}$$

2.3 Parameter sensitivity analysis

According to (3) and (6), DPCC is a model-based control and includes motor parameters such as the stator resistance, d–q-axis inductances, and rotor flux. This indicates that the DPCC is parameter-sensitive and that the accuracy of the system model affects the current control performance. Therefore it is necessary to analyse the performance of the current control when the parameters are mismatched.

To drive the motor in an actual system, the parameter is measured offline, and the value of the parameter estimated by the measurement error may differ from the actual parameter value of the motor. The predictive model of the stator current with a

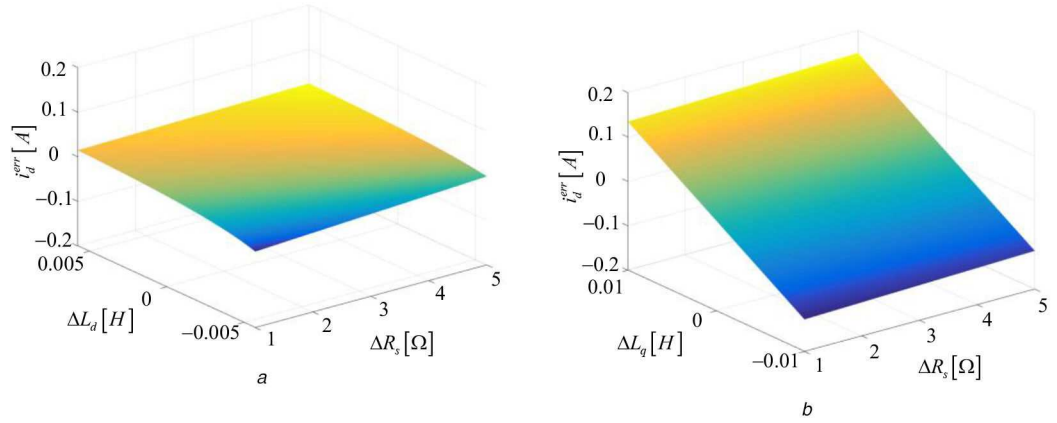

Fig. 1 *d-axis current prediction errors of conventional predictive control at 1500 r/min and under 1.6 N m conditions*
(a) With a mismatch of the *d*-axis inductance and resistance, ***(b)*** With a mismatch of the *q*-axis inductance and resistance

mismatch of the actual parameter value can be expressed as (7) using (3) and (4).

$$\begin{cases} i_d^{\Delta}(k+1) = \left[1 - \dfrac{T_s(R_s + \Delta R_s)}{(L_d + \Delta L_d)}\right] i_d(k) + \dfrac{T_s}{(L_d + \Delta L_d)} v_d(k) \\ \qquad + \dfrac{T_s(L_q + \Delta L_q)}{(L_d + \Delta L_d)} \omega_r(k) i_q(k) \\ i_q^{\Delta}(k+1) = \left[1 - \dfrac{T_s(R_s + \Delta R_s)}{(L_q + \Delta L_q)}\right] i_q(k) + \dfrac{T_s}{(L_q + \Delta L_q)} v_q(k) \\ \qquad - \dfrac{T_s(L_d + \Delta L_d)}{(L_q + \Delta L_q)} \omega_r(k) i_d(k) \\ \qquad - \dfrac{T_s(\lambda_m + \Delta\lambda_m)}{(L_q + \Delta L_q)} \omega_r(k) \end{cases} \quad (7)$$

where ΔR_s, ΔL_d, ΔL_q, and $\Delta\lambda_m$ are the errors between the actual parameter value and the estimated parameter value, and $i_d^{\Delta}(k+1)$ $i_q^{\Delta}(k+1)$ are the *d*–*q*-axis predicted currents owing to a parameter mismatch.

The prediction errors from a parameter mismatch can be obtained based on the difference between (3) and (7) and are shown in (see (8)) , where $i_d^{err}(k+1)$ and $i_q^{err}(k+1)$ are the *d*–*q*-axis predicted current errors owing to parameter mismatch, respectively.

From (8), it can be seen that the rotor flux mismatch only affects i_q, and that the stator resistance and *d*–*q*-axis inductance mismatch affect both i_d and i_q.

Fig. 1 shows the relationship between each parameter mismatch and the *d*-axis prediction error. As can be seen in Fig. 1*a*, the *d*-axis prediction error is not significantly affected by the mismatch between stator resistance and *d*-axis inductance. However, Fig. 1*b* shows the mismatch with the *q*-axis inductance has a significant effect on the *d*-axis prediction error.

Fig. 2 shows the relationship between each parameter mismatch and the *q*-axis prediction error. As can be seen in Fig. 2*a*, the *q*-axis prediction error is not greatly affected by the mismatch between stator resistance and *d*-axis inductance. Fig. 2*b* shows that *q*-axis prediction error is slightly affected by the variation of stator resistance and *q*-axis inductance. In addition, Fig. 2*c* shows the mismatch with the rotor flux has a significant effect on the *q*-axis prediction error. Therefore, as can be seen in Figs. 1 and 2, a robust control method is required, particularly for the *q*-axis inductance and rotor flux mismatched.

3 Novel RPCC with proposed disturbance observer in discrete-time domain

The parameter mismatch in the conventional DPCC degrades the performance of the current control. A disturbance estimation is necessary for the predictive current controller to operate robustly to the parameters.

The Luenberger observer can compensate for deviations between the actual system and the model used for control, and can be applied to eliminate disturbance effects and noise. To eliminate a disturbance owing to an uncertainty of the system, the estimated disturbance in the observer is applied as a feedforward compensation to the predicted reference voltage considering the digital delay.

3.1 Novel predictive discrete-time model with disturbances

If the nominal parameter value is used, and uncertainty owing to parameter mismatch is taken into the dynamic disturbance, a novel

$$\begin{cases} i_d^{err} = \left[\dfrac{T_s(R_s\Delta L_d - \Delta R_s L_d)}{L_d(L_d + \Delta L_d)}\right] i_d(k) \\ \qquad + \left[\dfrac{T_s(L_d\Delta L_q - L_q\Delta L_d)}{L_d(L_d + \Delta L_d)}\right] \omega_r(k) i_q(k) \\ \qquad - \left[\dfrac{T_s\Delta L_d}{L_d(L_d + \Delta L_d)}\right] v_d(k) \\ i_q^{err} = \left[\dfrac{T_s(R_s\Delta L_q - \Delta R_s L_q)}{L_q(L_q + \Delta L_q)}\right] i_q(k) \\ \qquad + \left[\dfrac{T_s(L_d\Delta L_q - L_q\Delta L_d)}{L_q(L_q + \Delta L_q)}\right] \omega_r(k) i_d(k) \\ \qquad - \left[\dfrac{T_s\Delta L_q}{L_q(L_q + \Delta L_q)}\right] v_q(k) \\ \qquad + \left[\dfrac{T_s(\lambda_m\Delta L_q - L_q\Delta\lambda_m)}{L_q(L_q + \Delta L_q)}\right] \omega_r(k) \end{cases} \quad (8)$$

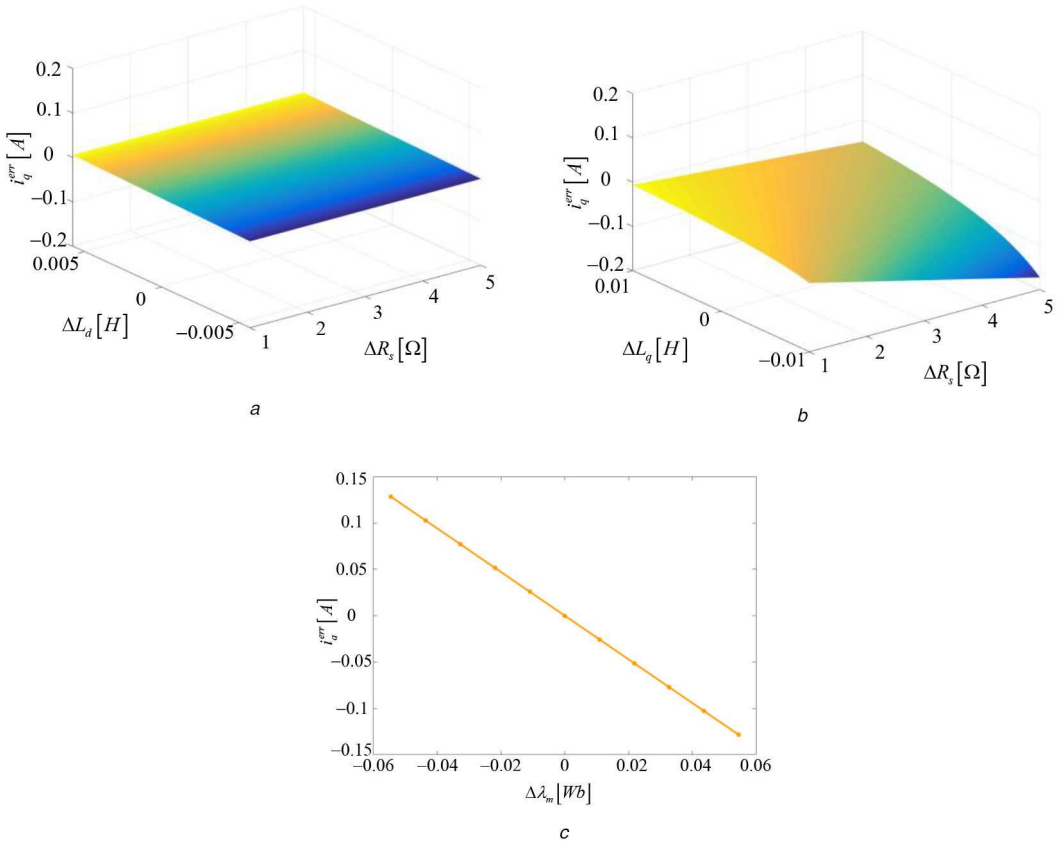

Fig. 2 *q-axis current prediction errors of conventional predictive control at 1500 r/min and under 1.6 N m conditions*
(a) With a mismatch of the *d*-axis inductance and resistance, ***(b)*** With a mismatch of the *q*-axis inductance and resistance, ***(c)*** With a mismatch of the rotor flux

stator voltage model for IPMSM with disturbance terms can be rewritten as

$$\begin{cases} v_d = R_{sn} i_d + L_{dn} \dfrac{\mathrm{d}i_d}{\mathrm{d}t} - L_{qn} \omega_{\mathrm{r}} i_q + f_d \\ v_q = R_{sn} i_q + L_{qn} \dfrac{\mathrm{d}i_q}{\mathrm{d}t} + L_{dn} \omega_{\mathrm{r}} i_d + f_q \end{cases} \tag{9}$$

where the subscript 'n' denotes the nominal value, and f_d and f_q are expressed using (10).

$$\begin{cases} f_d = \Delta R_{\mathrm{s}} i_d + \Delta L_d \dfrac{\mathrm{d}i_d}{\mathrm{d}t} - \Delta L_q \omega_{\mathrm{r}} i_q + d_d \\ f_q = \Delta R_{\mathrm{s}} i_q + \Delta L_q \dfrac{\mathrm{d}i_q}{\mathrm{d}t} + \Delta L_d \omega_{\mathrm{r}} i_d + \lambda_{\mathrm{m}} \omega_{\mathrm{r}} + d_q \end{cases} \tag{10}$$

where $\Delta R_{\mathrm{s}} = R_{\mathrm{s}} - R_{sn}$, $\Delta L_d = L_d - L_{dn}$, $\Delta L_q = L_q - L_{qn}$, and d_d and d_q represent unmodelled dynamics.

It should be noted that f_d and f_q are not state variables but disturbances caused by parameter variations or other unstructured uncertainties. In addition, by adding a rotor flux and the rotor speed term to the q-axis disturbance term as shown in (10), state variables in (9) independent of the rotor flux are derived. The voltage (9) including the disturbance components can be expressed as a discrete-time model matrix, as shown in (11). Here, $\boldsymbol{A}_n$ and $\boldsymbol{B}_n$ are control matrices containing nominal IPMSM parameters and are given by (12). Therefore, a novel predictive discrete-time stator voltage model independent of the rotor flux term of IPMSM can be obtained by

$$\begin{bmatrix} v_d(k) \\ v_q(k) \end{bmatrix} = \boldsymbol{B}_n^{-1} \left\{ \begin{bmatrix} i_d(k+1) \\ i_q(k+1) \end{bmatrix} - \boldsymbol{A}_n(k) \begin{bmatrix} i_d(k) \\ i_q(k) \end{bmatrix} \right\} + \begin{bmatrix} f_d(k) \\ f_q(k) \end{bmatrix} \tag{11}$$

$$\boldsymbol{A}_n(k) = \begin{bmatrix} 1 - \dfrac{T_{\mathrm{s}} R_{sn}}{L_{dn}} & \dfrac{L_{qn}}{L_{dn}} T_{\mathrm{s}} \omega_{\mathrm{r}}(k) \\ -\dfrac{L_{dn}}{L_{qn}} T_{\mathrm{s}} \omega_{\mathrm{r}}(k) & 1 - \dfrac{T_{\mathrm{s}} R_{sn}}{L_{qn}} \end{bmatrix}$$
$$\boldsymbol{B}_n = \begin{bmatrix} \dfrac{T_{\mathrm{s}}}{L_{dn}} & 0 \\ 0 & \dfrac{T_{\mathrm{s}}}{L_{qn}} \end{bmatrix}. \tag{12}$$

The predicted currents $i_d(k+1)$ and $i_q(k+1)$ can be easily computed using the present sampled values from (11) in the following equation

$$\begin{bmatrix} i_d(k+1) \\ i_q(k+1) \end{bmatrix} = \boldsymbol{A}_n(k) \begin{bmatrix} i_d(k) \\ i_q(k) \end{bmatrix} + \boldsymbol{B}_n \begin{bmatrix} v_d(k) - f_d(k) \\ v_q(k) - f_q(k) \end{bmatrix}. \tag{13}$$

To apply deadbeat control, as shown in (6), the matrix for the reference voltage including the disturbance terms can be expressed as

$$\begin{bmatrix} v_d^{\mathrm{ref}}(k) \\ v_q^{\mathrm{ref}}(k) \end{bmatrix} = \boldsymbol{B}_n^{-1} \left\{ \begin{bmatrix} i_d^{\mathrm{ref}}(k+1) \\ i_q^{\mathrm{ref}}(k+1) \end{bmatrix} - \boldsymbol{A}_n(k) \begin{bmatrix} i_d(k) \\ i_q(k) \end{bmatrix} \right\} + \begin{bmatrix} f_d(k) \\ f_q(k) \end{bmatrix}. \tag{14}$$

In real digital implementations, the update mechanism of the microprocessor is applied with an inherent delay. As a result, the voltage vector selected at the (k)th instant is not a voltage vector minimising the current error in the next period, which leads to poor control performance. Assuming that a one-period delay occurs from a digital control, the control delay can be compensated using the predicted values after two periods from the present state. Thus, assuming that (14) moves after one period, and the current

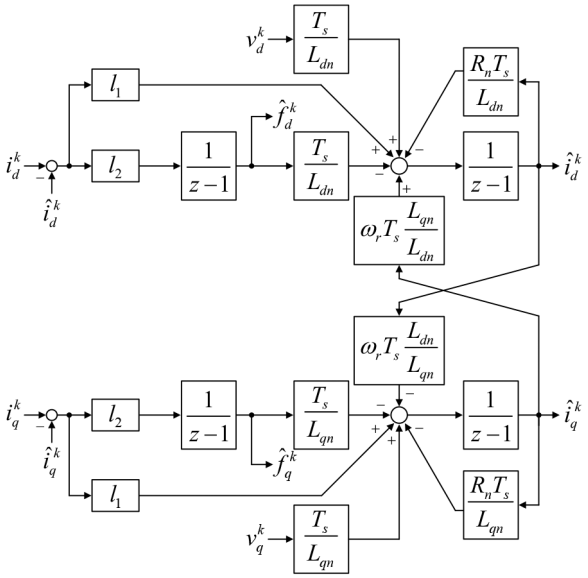

Fig. 3 *Block diagram of DOB in the discrete-time domain*

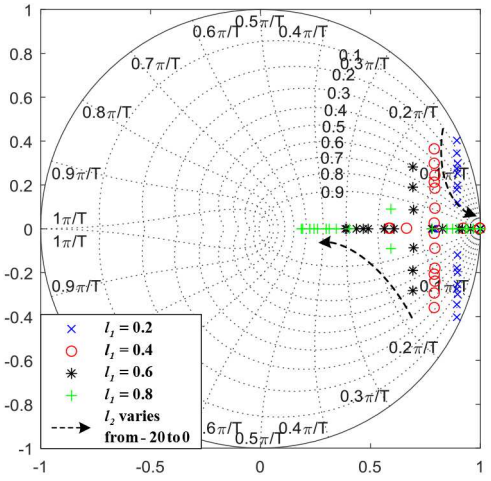

Fig. 4 *Closed-loop pole loci of the DOB with l_1 varied between 0.2 and 0.8, and l_2 varied between − 20 and 0*

reference $\left(i_{dq}^{\text{ref}}(k) = i_{dq}^{\text{ref}}(k+1) = i_{dq}^{\text{ref}}(k+2)\right)$ is constant, the predicted reference voltage can be expressed as

$$\begin{bmatrix} v_d^{\text{ref}}(k+1) \\ v_q^{\text{ref}}(k+1) \end{bmatrix} = \boldsymbol{B}_n^{-1}\left\{ \begin{bmatrix} i_d^{\text{ref}}(k) \\ i_q^{\text{ref}}(k) \end{bmatrix} - \boldsymbol{A}_n(k) \begin{bmatrix} i_d(k+1) \\ i_q(k+1) \end{bmatrix} \right\} + \begin{bmatrix} f_d(k+1) \\ f_q(k+1) \end{bmatrix} \tag{15}$$

where $v_d^{\text{ref}}(k+1)$ and $v_q^{\text{ref}}(k+1)$ are the d–q-axis $(k+1)$th predicted reference voltages, respectively.

From (15), future disturbances $f_d(k+1)$ and $f_q(k+1)$ can be estimated as (16) using the Lagrange interpolation formula [26]

$$\begin{bmatrix} f_d(k+1) \\ f_q(k+1) \end{bmatrix} = 3\begin{bmatrix} f_d(k) \\ f_q(k) \end{bmatrix} - 3\begin{bmatrix} f_d(k-1) \\ f_q(k-1) \end{bmatrix} + \begin{bmatrix} f_d(k-2) \\ f_q(k-2) \end{bmatrix}. \tag{16}$$

3.2 Design of discrete-time disturbance observer

For the RPCC, a disturbance estimation is necessary. Assuming that the disturbance values are constant during the sampling period, the state-space equation with disturbance terms can be obtained using (13). Here, $\boldsymbol{\Phi}$, $\boldsymbol{\Gamma}$, and $\boldsymbol{I}$ are given by (18).

$$\begin{bmatrix} i_d(k+1) \\ i_q(k+1) \\ f_d(k+1) \\ f_q(k+1) \end{bmatrix} = \boldsymbol{\Phi}\begin{bmatrix} i_d(k) \\ i_q(k) \\ f_d(k) \\ f_q(k) \end{bmatrix} + \boldsymbol{\Gamma}\begin{bmatrix} v_d(k) \\ v_q(k) \\ 0 \\ 0 \end{bmatrix} \tag{17}$$

$$\boldsymbol{\Phi} = \begin{bmatrix} \boldsymbol{A}_n(k) & -\boldsymbol{B}_n \\ 0 & \boldsymbol{I} \end{bmatrix}, \quad \boldsymbol{\Gamma} = \begin{bmatrix} \boldsymbol{B}_n & 0 \\ 0 & 0 \end{bmatrix}, \quad \boldsymbol{I} = \begin{bmatrix} 1 & 0 \\ 0 & 1 \end{bmatrix}. \tag{18}$$

From (17), the DOB can be constructed as shown in (19), and the observer gains (l_1, l_2) are designed using a pole placement method.

$$\begin{bmatrix} \hat{i}_d(k+1) \\ \hat{i}_q(k+1) \\ \hat{f}_d(k+1) \\ \hat{f}_q(k+1) \end{bmatrix} = \boldsymbol{\Phi}\begin{bmatrix} \hat{i}_d(k) \\ \hat{i}_q(k) \\ \hat{f}_d(k) \\ \hat{f}_q(k) \end{bmatrix} + \boldsymbol{\Gamma}\begin{bmatrix} v_d(k) \\ v_q(k) \\ 0 \\ 0 \end{bmatrix} + \boldsymbol{L}\left\{ \begin{bmatrix} i_d(k) \\ i_q(k) \\ i_d(k) \\ i_q(k) \end{bmatrix} - \boldsymbol{H}\begin{bmatrix} \hat{i}_d(k) \\ \hat{i}_q(k) \\ \hat{f}_d(k) \\ \hat{f}_q(k) \end{bmatrix} \right\} \tag{19}$$

where $\boldsymbol{L} = \begin{bmatrix} l_1\boldsymbol{I} & 0 \\ 0 & l_2\boldsymbol{I} \end{bmatrix}$, and $\boldsymbol{H} = \begin{bmatrix} \boldsymbol{I} & 0 \\ \boldsymbol{I} & 0 \end{bmatrix}$.

Fig. 3 shows a block diagram of the DOB in the discrete-time domain. This DOB represents the characteristics of the system, and the estimated state converges to the actual state under the same currents and voltages applied in the actual system. Therefore, the proposed observer can estimate the disturbance components with the appropriate gain using the estimation error of the state variable. In addition, this observer is configured with nominal values and can be designed without a rotor flux term. The outputs ($\hat{f}_d(k)$ and $\hat{f}_q(k)$) of the observer are generated through a parameter mismatch, rotor flux linkage, and unmodelled dynamics, and are compensated with the predicted reference voltage in (15).

3.3 Stability analysis

The stability analysis of the proposed DOB can be performed by mapping the closed-loop poles of the system. The closed-loop characteristic equation of the DOB can be obtained using

$$\det\left[z\boldsymbol{I} - (\boldsymbol{\Phi} - \boldsymbol{L}\boldsymbol{H})\right] = 0. \tag{20}$$

To simplify the stability analysis, the cross-coupling term in Fig. 3 is omitted because it is extremely small.

According to (20), the observer characteristic equation is derived in the Appendix. Fig. 4 shows the closed-loop poles loci of the DOB, where l_1 changes from 0.2 to 0.8 and l_2 changes from −20 to 0. As shown in Fig. 4, the observer is stable when l_1 is above 0.2 and l_2 is below zero. However, observer gains need to be set appropriately because they affect the bandwidth and damping ratio. In this paper, observer gains are selected as $l_1 = 0.4$ and $l_2 = -10$.

To evaluate the effects of a parameter mismatch on the DOB, closed-loop poles loci were analysed for a variation of the nominal values of L_{dn}, L_{qn}, and R_{sn}. Figs. 5*a* and *b* show the closed-loop poles loci when the nominal values of the d–q-axis inductance are varied from 50 to 150% of the actual d–q-axis inductance values $(L_d = 11.5\,\text{mH},\ L_q = 20\,\text{mH})$. Fig. 5*c* shows the closed-loop poles loci when the nominal value of the stator resistance is varied from 0 to 10 Ω. As shown in Fig. 5, the closed-loop poles of the DOB exist in the unit circle, and the system is stable. As the nominal

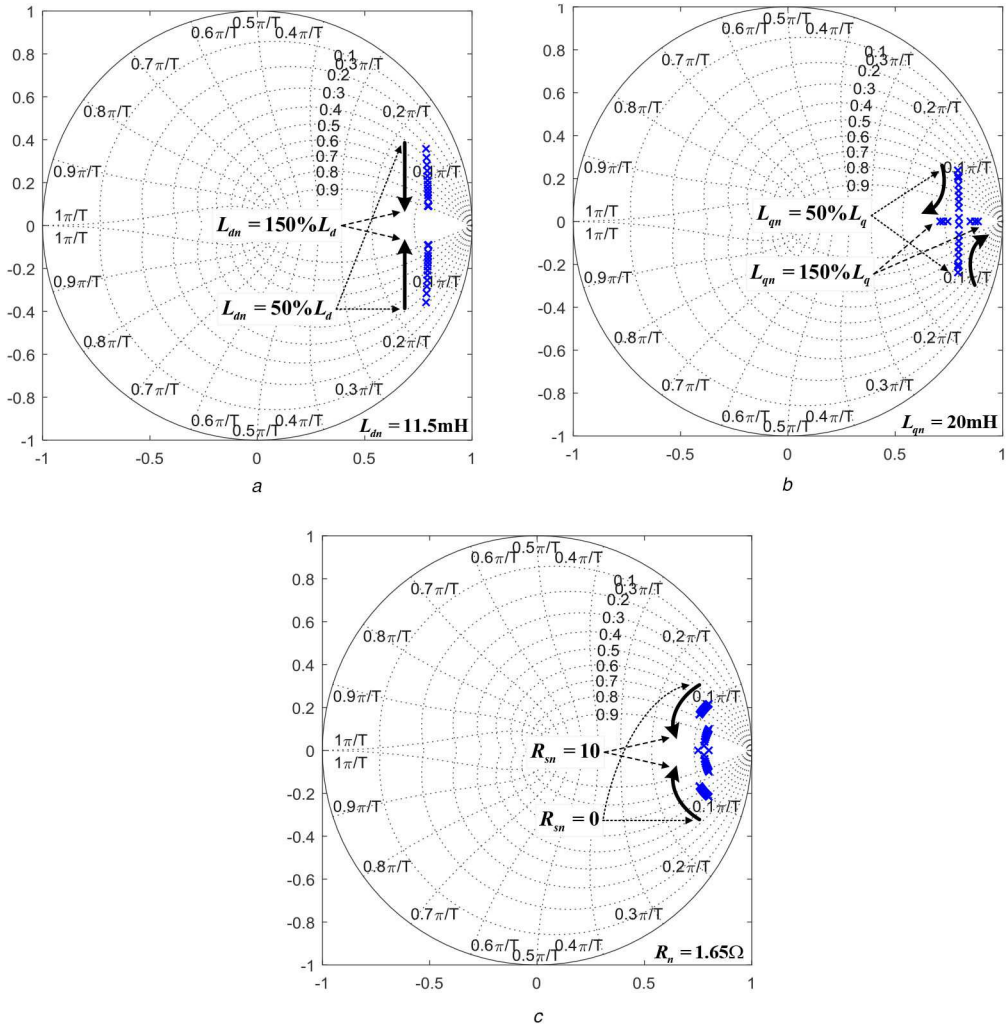

Fig. 5 *Closed-loop pole loci of the DOB with parameter variations*
(a) L_{dn} varied from 50 to 150% of the actual value, ***(b)*** L_{qn} varied from 50 to 150% of the actual value, ***(c)*** R_{sn} varied from 0 to 10 Ω

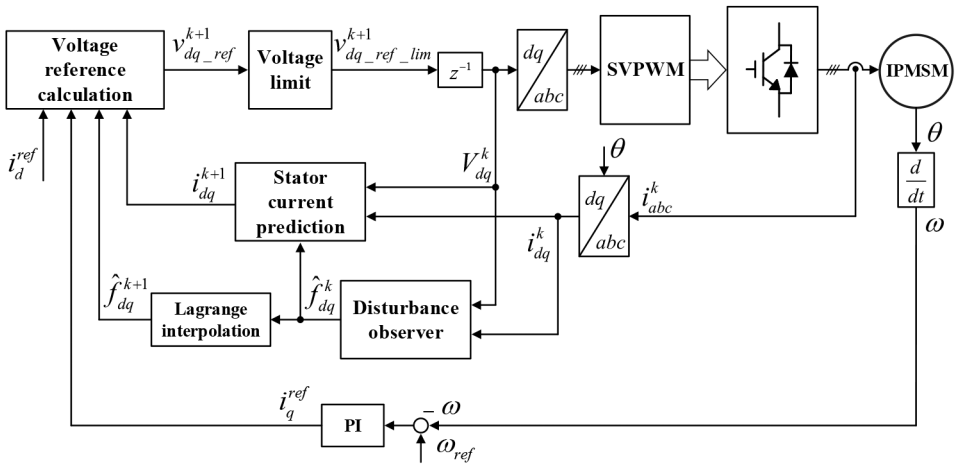

Fig. 6 *Block diagram of the RPCC with proposed DOB*

value is smaller than the actual value, the damping ratio decreases and the pole becomes unstable because it will be close to the unit circle. In contrast, as the nominal value becomes larger than the actual value, the damping ratio increases and the system does not diverge.

Fig. 6 shows the entire control block diagram including the proposed DOB for an RPCC.

In the proposed scheme, the control block diagram is composed of a PI speed controller, DOB, Lagrange interpolation, stator current prediction, and voltage reference calculation. The outputs of the DOB go into the stator current prediction block and Langrange interpolation. The voltage reference calculation block outputs the predicted reference voltages compensated for the disturbance term considering a digital delay.

Figs. 7 and 8 show the relationship between each parameter mismatch and the *d*–*q*-axis prediction error. In contrast to Figs. 1 and 2, using the proposed method, there are almost no *d*–*q*-axis predicted current errors for all parameters. Therefore, the proposed method is robust to the parameter variations.

To verify the effectiveness of the proposed method, experiments were conducted on the prototype of the IPMSM system. The parameters of the IPMSM are shown in Table 1.

4 Experimental results

The proposed control method is implemented in an experimental system using a DSP TMS320F28335 in which the PWM switching frequency is 10 kHz. To clearly demonstrate the current level, the *d*-axis reference current is set to 0 A in the experiment, and the *q*-axis current is set as the speed controller output value. The gains of the proposed Luenberger observer are selected as $l_1 = 0.4$ and $l_2 = -10$, as described in the previous section.

To evaluate the validity of the proposed current control method under a motor parameter mismatch in a steady-state condition, we compared the experimental results of the proposed RPCC with a conventional DPCC. The experiment was conducted at a full load of 1.6 Nm and at 1500 r/min. Stator resistance R_s, *d*-axis

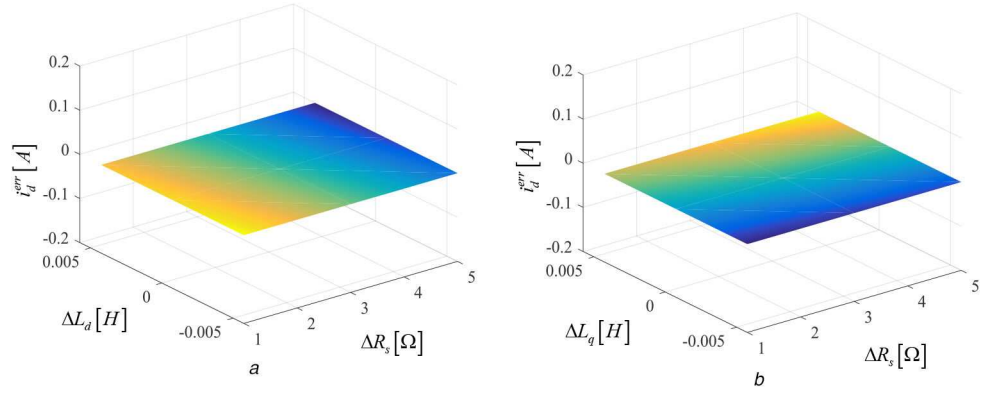

Fig. 7 *d-axis current prediction errors of proposed predictive control at 1500 r/min and under 1.6 N m conditions*
(a) With a mismatch of the *d*-axis inductance and resistance, ***(b)*** With a mismatch of the *q*-axis inductance and resistance

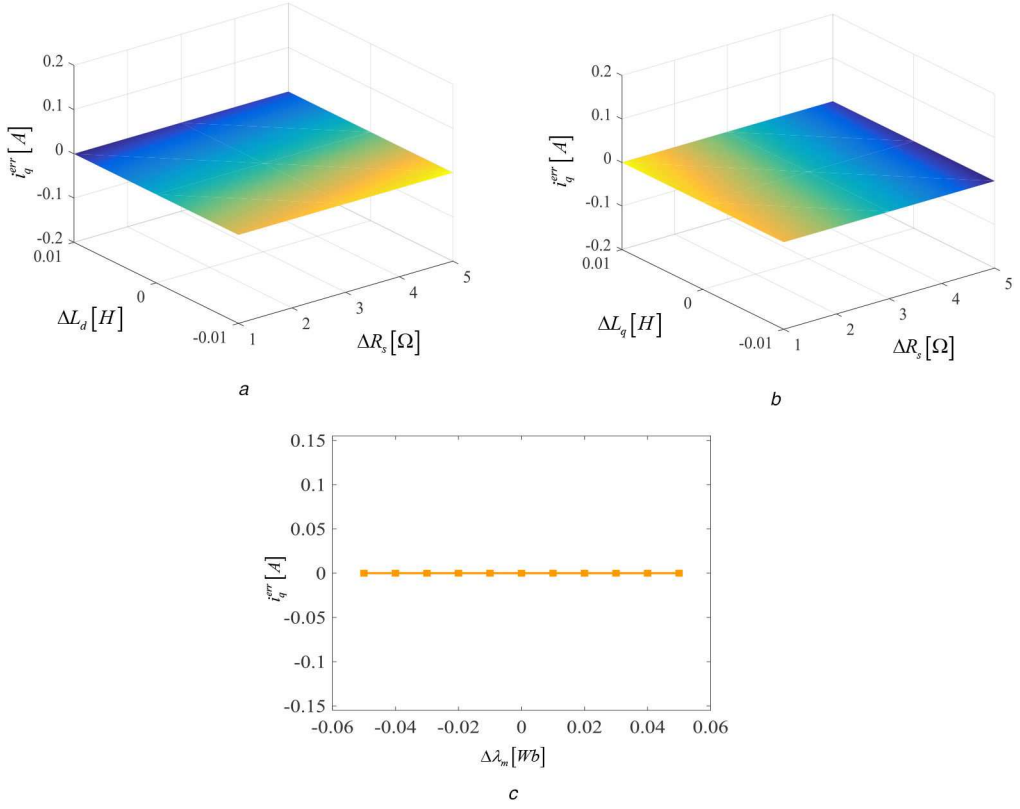

Fig. 8 *q-axis current prediction errors of proposed predictive control at 1500 r/min and under 1.6 N m conditions*
(a) With a mismatch of the *d*-axis inductance and resistance, ***(b)*** With a mismatch of the *q*-axis inductance and resistance, ***(c)*** With a mismatch of the rotor flux

Table 1 Motor parameters

Parameter	Value	Unit
rated power	600	W
rated torque	1.6	N m
pole pairs	3	—
stator resistance	1.65	Ω
d-axis inductance	11.5	mH
q-axis inductance	20	mH
permanent magnet flux linkage	0.105	Wb
DC-link voltage	311	V

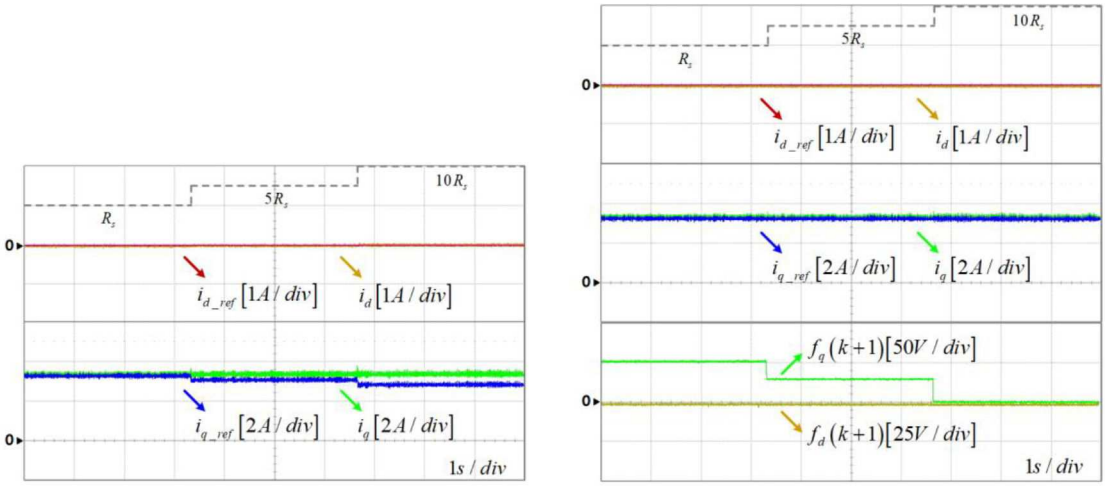

a b

Fig. 9 *Experimental results under R_s mismatch*
(a) Conventional DPCC, ***(b)*** RPCC with proposed DOB

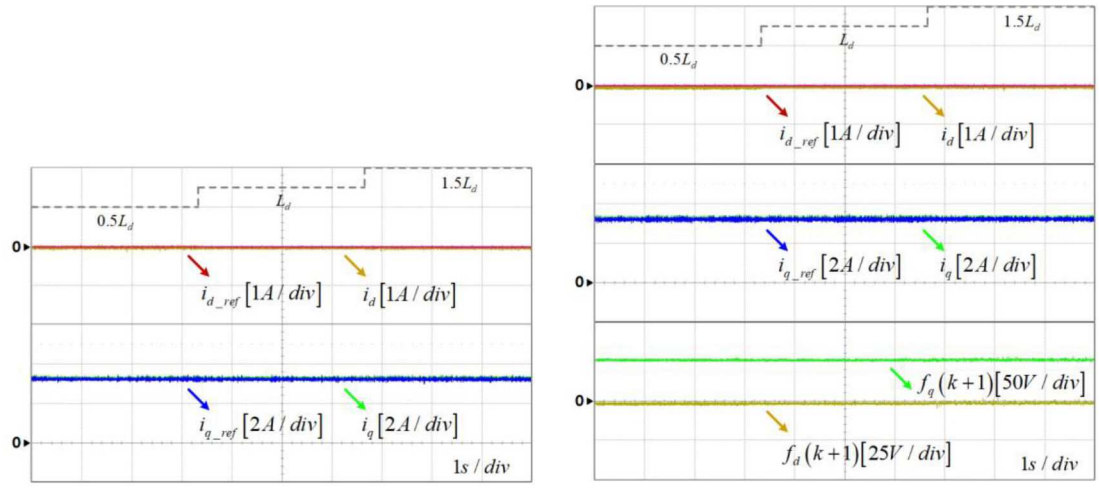

a b

Fig. 10 *Experimental results under L_d mismatch*
(a) Conventional DPCC, ***(b)*** RPCC with proposed DOB

inductance L_d, q-axis inductance L_q, and rotor flux λ_m were chosen as the test motor parameters. The performance of the current control to the parameter variation was confirmed by changing the parameters of the current controller programming code into three steps in online. The experimental waveforms include the d–q-axis reference currents and d–q-axis currents, and the estimated disturbance terms $f_d(k+1)$, $f_q(k+1)$ are also given in the proposed method.

Fig. 9 shows the current response of the conventional DPCC and the proposed scheme under R_s mismatch. The parameter step change of R_s is $R_s = R_s \rightarrow 5 \cdot R_s \rightarrow 10 \cdot R_s$.

As shown in Fig. 9*a*, the d-axis current follows the reference value well in a conventional DPCC; however, owing to a mismatch of the stator resistance, the q-axis current fails to follow the reference value accurately, and an error occurs. A conventional DPCC is somewhat sensitive to the stator resistance. In contrast, as shown in Fig. 9*b*, $f_d(k+1)$ and $f_q(k+1)$ of the proposed method compensate the steady-state current error caused by a mismatch of the stator resistance, and all d–q-axis currents follow their reference values well.

Fig. 10 shows the current response of the conventional DPCC and the proposed scheme under L_d mismatch. The parameter step change of L_d is $L_d = 0.5 \cdot L_d \rightarrow L_d \rightarrow 1.5 \cdot L_d$. As shown in Fig. 10, both the current responses of the conventional DPCC and the proposed method follow their reference value well, even if L_d mismatch occurs. Therefore, as shown in Figs. 1 and 2, the conventional DPCC and the proposed method are not sensitive to the influence of L_d.

Fig. 11 shows the current response of the conventional DPCC and the proposed scheme under L_q mismatch. The parameter step change of L_q is $L_q = 0.5 \cdot L_q \rightarrow L_q \rightarrow 1.5 \cdot L_q$. As shown in Fig. 11*a*, the q-axis current follows the reference value well in the conventional DPCC; however, owing to a mismatch of the q-axis inductance, the d-axis current fails to follow the reference value accurately, and an error occurs.

A conventional DPCC is sensitive to the q-axis inductance. However, as shown in Fig. 11*b*, $f_d(k+1)$ and $f_q(k+1)$ of the proposed method compensate the steady-state current error caused by a mismatch of the q-axis inductance, and all d–q-axis currents follow their reference values well.

Fig. 12 shows the current response of a conventional DPCC and the proposed scheme under a λ_m mismatch.

The parameter step change of λ_m is $\lambda_m = 0 \rightarrow \lambda_m \rightarrow 2 \cdot \lambda_m$. As shown in Fig. 12*a*, the d-axis current follows the reference value well; however, owing to the mismatch of the rotor flux, in a conventional DPCC, the q-axis current does not follow the reference value correctly, and an error occurs. A conventional DPCC is sensitive to the rotor flux. In contrast, as shown in Fig. 12*b*, even though the rotor flux is zero because $f_q(k+1)$ of the proposed method already includes the value of λ_m and compensates for the steady-state current error, all d–q-axis currents follow their reference values well. Therefore, the proposed method does not

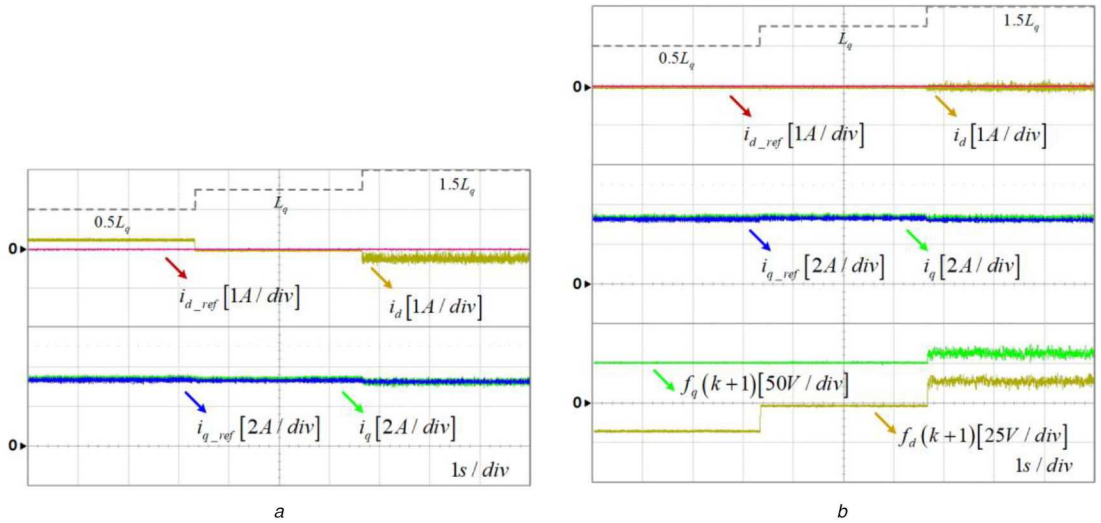

a *b*

Fig. 11 *Experimental results under L_q mismatch*
(a) Conventional DPCC, ***(b)*** RPCC with proposed DOB

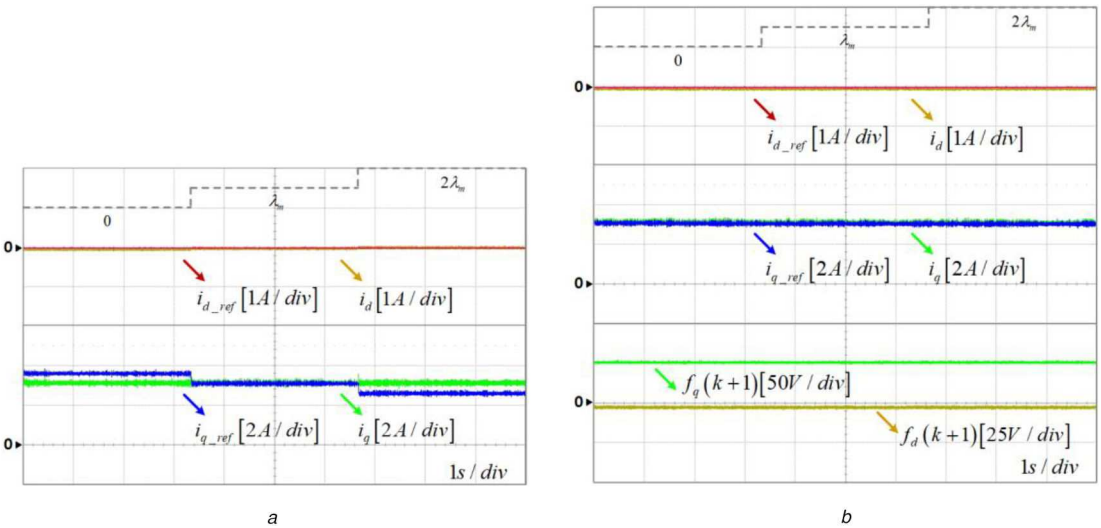

a *b*

Fig. 12 *Experimental results under λ_m mismatch*
(a) Conventional DPCC, ***(b)*** RPCC with proposed DOB

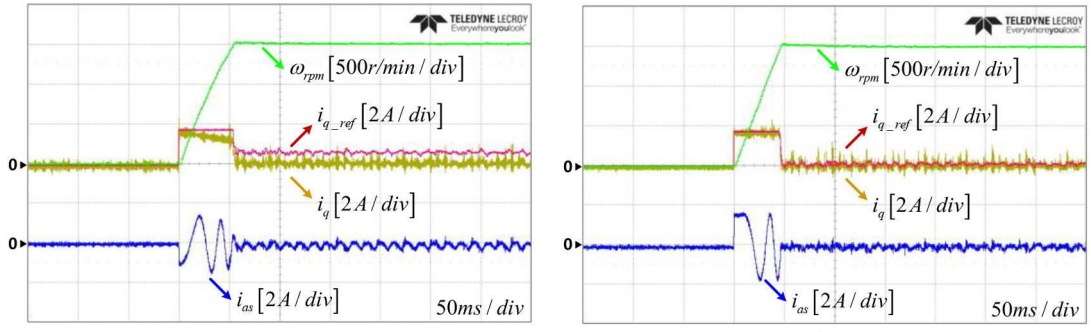

a *b*

Fig. 13 *Starting responses from standstill to 1500 r/min under λ_{mn} = 0*
(a) Conventional DPCC, ***(b)*** RPCC with proposed DOB

require the rotor flux information, and accurate current control is possible.

To evaluate the validity of the proposed current control method under a motor parameter mismatch in a transient condition, transient experiments were performed on starting and speed reversal to confirm the independence of rotor flux information.

Fig. 13 shows the starting responses of the motor speed, *q*-axis current reference, *q*-axis current, and the stator current in the *abc* frame from standstill to 1500 r/min when the rotor flux is 0. As shown in Fig. 13*a*, when the rotor flux is 0, the feedforward term of the motor stator voltage equation disappears. As a result, the output voltage becomes small during acceleration, so undercurrent of *q*-axis current occurs in the transient state. Therefore, the desired torque cannot be obtained and the acceleration of the motor is slow. On the other hand, in Fig. 13*b*, even though the rotor flux is 0 because the voltage compensation by the proposed method is performed to the motor stator voltage equation as shown in (15), an appropriate *q*-axis current response can be obtained. Therefore, it is possible to obtain an appropriate torque and to accelerate a little faster than Fig. 13*a*.

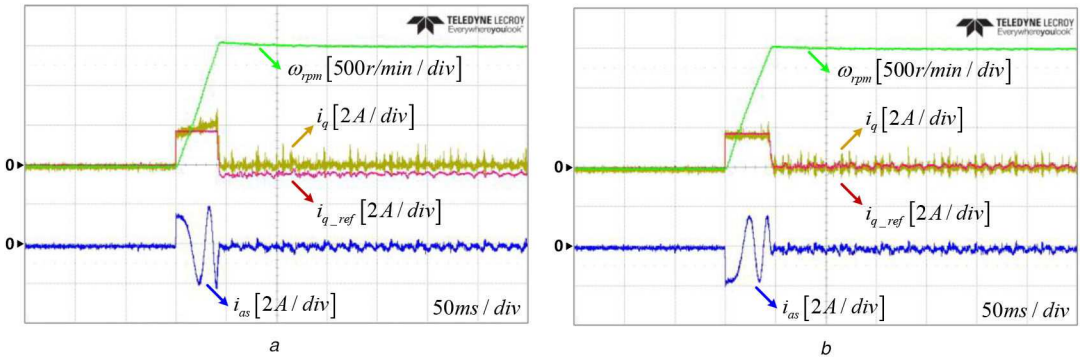

Fig. 14 *Starting responses from standstill to 1500 r/min under $\lambda_{mn} = 2 \cdot \lambda_m$*
(a) Conventional DPCC, ***(b)*** RPCC with proposed DOB

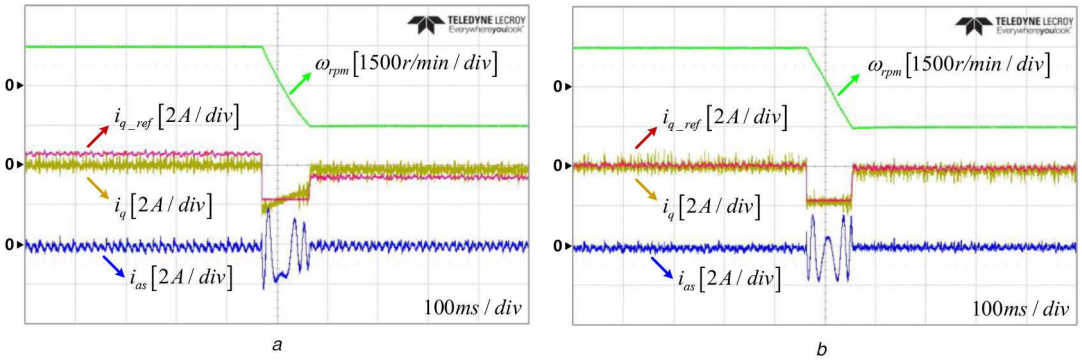

Fig. 15 *Forward-Revese speed control from 1500 to -1500 r/min under $\lambda_{mn} = 0$*
(a) Conventional DPCC, ***(b)*** RPCC with proposed DOB

Fig. 14 shows the starting responses of the motor speed, q-axis current reference, q-axis current, and the stator current in the abc frame from standstill to 1500 r/min when the nominal value of rotor flux is twice the actual value. As shown in Fig. 14*a*, when the nominal value of rotor flux is twice the actual value, the feedforward term of the motor stator voltage equation is doubled. As a result, the output voltage becomes large during acceleration, so overcurrent of q-axis current occurs in the transient state. Therefore, the motor will accelerate faster because it outputs a torque greater than the desired torque. Accordingly, a speed overshoot occurs and it is difficult to satisfy the desired speed response. On the other hand, in Fig. 14*b*, even though nominal value of rotor flux is twice the actual value because the voltage compensation by the proposed method is performed to the motor stator voltage equation as shown in (15), an appropriate q-axis current response can be obtained. Therefore, it is possible to obtain an appropriate torque and speed response.

Fig. 15 shows the results of speed reversal operation at ±1500 r/min when the rotor flux is 0. As shown in Fig. 15*a*, due to the absence of an accurate feedforward value, an error occurs in the output voltage, resulting in a current error in the region where the speed changes abruptly. Therefore, a linear speed change cannot be obtained. On the other hand, in Fig. 15*b*, the proposed method improves the current control without the information of the rotor flux, and thus achieves a linear speed response.

The experimental results show that the current error is not large for L_d mismatch, and the mismatch between L_q and λ_m significantly affects the predicted current error, that is similar to Figs. 1 and 2. In the case of R_s, a current error occurs when the degree of mismatch is large. The proposed method can compensate for R_s, L_d, L_q and λ_m parameter errors to obtain a more accurate current control response.

5 Conclusion

In this paper, RPCC for an IPMSM without rotor flux information based on a discrete-time DOB was proposed. Deadbeat control and model-based predictive current control predict a current using the model of the motor and generate the predicted reference voltage, and thus the current control performance is considered to be parameter sensitive. The current control error according to the parameter variation was analysed. Therefore, a discrete-time DOB based on a Luenberger observer with a robust parameter variation was proposed for accurate current control, and the estimated disturbances are compensated with the predicted voltage reference model considering a digital delay. Compared with a conventional DPCC, the proposed method is robust against variations of R_s, L_d, and L_q, and accurate current control can be obtained even without information on λ_m. Therefore, the proposed method is robust to the parameters, and there is no need for a parameter estimation technique to estimate the rotor flux either offline or online. To verify the validity of the proposed method, experimental results compared with a conventional DPCC are presented under the IPMSM parameter mismatch conditions.

6 References

[1] Dey, A., Azeez, N.A., Mathew, K., *et al.*: 'Hysteresis current controller for a general n-level inverter fed drive with online current error boundary computation and nearly constant switching frequency', *IET Power Electron.*, 2013, **6**, (8), pp. 1640–1649

[2] Tiwari, A.N., Agarwal, P., Srivastava, S.P.: 'Performance investigation of modified hysteresis current controller with the permanent magnet synchronous motor drive', *IET Electr. Power Appl.*, 2010, **4**, (2), pp. 101–108

[3] Casadei, D., Profumo, F., Serra, G., *et al.*: 'FOC and DTC: two viable schemes for induction motors torque control', *IEEE Trans. Power Electron.*, 2002, **17**, (5), pp. 779–787

[4] Buja, G.S., Kazmierkowski, M.P.: 'Direct torque control of PWM inverter-fed AC motors—A survey', *IEEE Trans. Ind. Electron.*, 2004, **51**, (4), pp. 744–757

[5] Morel, F., Xuefang, L.S., Rétif, J.M., *et al.*: 'A comparative study of predictive current control schemes for a permanent-magnet synchronous machine drive', *IEEE Trans. Ind. Electron.*, 2009, **56**, (7), pp. 2715–2728

[6] Shi, T., Xu, Y., Xiao, M., *et al.*: 'VSP predictive torque control of PMSM', *IET Electr. Power Appl.*, 2019, **13**, (4), pp. 463–471

[7] Rodríguez, J., Pontt, J., Silva, C.A., *et al.*: 'Predictive current control of a voltage source inverter', *IEEE Trans. Ind. Electron.*, 2007, **54**, (1), pp. 495–503

[8] Vazquez, S., Rodriguez, J., Rivera, M., *et al.*: 'Model predictive control for power converters and drives: advances and trends', *IEEE Trans. Ind. Electron.*, 2017, **64**, (2), pp. 935–947

[9] Chen, Y., Liu, T.H., Hsiao, C.F., *et al.*: 'Implementation of adaptive inverse controller for an interior permanent magnet synchronous motor adjustable

speed drive system based on predictive current control', *IET Electr. Power Appl.*, 2015, **9**, (1), pp. 60–70
[10] Chen, Z., Qiu, J., Jin, M.: 'Adaptive finite-control-set model predictive current control for IPMSM drives with inductance variation', *IET Electr. Power Appl.*, 2017, **11**, (5), pp. 874–884
[11] Wang, T., Liu, C., Lei, G., *et al.*: 'Model predictive direct torque control of permanent magnet synchronous motors with extended set of voltage space vectors', *IET Electr. Power Appl.*, 2017, **11**, (8), pp. 1376–1382
[12] Springob, L., Holtz, J.: 'High-bandwidth current control for torque-ripple compensation in PM synchronous machines', *IEEE Trans. Ind. Electron.*, 1998, **45**, (5), pp. 713–721
[13] Bouafia, A., Gaubert, J.P., Krim, F.: 'Predictive direct power control of three-phase pulsewidth modulation (PWM) rectifier using space-vector modulation (SVM)', *IEEE Trans. Power Electron.*, 2010, **25**, (1), pp. 228–236
[14] Zhang, Y., Xie, W., Zhang, Y.: 'Deadbeat direct power control of three-phase pulse-width modulation rectifiers', *IET Power Electron.*, 2014, **7**, (6), pp. 1340–1346
[15] Lee, K.J., Park, B.G., Kim, R.Y., *et al.*: 'Robust predictive current controller based on a disturbance estimator in a three-phase grid-connected inverter', *IEEE Trans. Power Electron.*, 2012, **27**, (1), pp. 276–283
[16] Wang, B., Chen, X., Yu, Y., *et al.*: 'Robust predictive current control with online disturbance estimation for induction machine drives', *IEEE Trans. Power Electron.*, 2017, **32**, (6), pp. 4663–4674
[17] Moreno, J.C., Huerta, J.M.E., Gil, R.G., *et al.*: 'A robust predictive current control for three-phase grid-connected inverters', *IEEE Trans. Ind. Electron.*, 2009, **56**, (6), pp. 1993–2004
[18] Siami, M., Khaburi, D. A., Rodríguez, J.: 'Torque ripple reduction of predictive torque control for PMSM drives with parameter mismatch', *IEEE Trans. Power Electron.*, 2017, **32**, (9), pp. 7160–7168
[19] Kim, K.H., Youn, M.J.: 'A simple and robust digital current control technique of a PM synchronous motor using time delay control approach', *IEEE Trans. Power Electron.*, 2001, **16**, (1), pp. 72–82
[20] Kwak, S.S., Moon, U.C., Park, J.C.: 'Predictive-control-based direct power control with an adaptive parameter identification technique for improved AFE performance', *IEEE Trans. Power Electron.*, 2014, **29**, (11), pp. 6178–6187
[21] Nalakath, S., Preindl, M., Emadi, A.: 'Online multi-parameter estimation of interior permanent magnet motor drives with finite control set model predictive control', *IET Electr. Power Appl.*, 2017, **11**, (5), pp. 944–951
[22] Liu, K., Zhu, Z.Q.: 'Mechanical parameter estimation of permanent-magnet synchronous machines with aiding from estimation of rotor PM flux linkage', *IEEE Trans. Ind. Appl.*, 2015, **51**, (4), pp. 3115–3125
[23] Huerta, J.M.E., Moreno, J.C., Fischer, J.R., *et al.*: 'A synchronous reference frame robust predictive current control for three-phase grid-connected inverters', *IEEE Trans. Ind. Electron.*, 2010, **57**, (3), pp. 954–962
[24] Pillay, P., Krishnan, R.: 'Modeling of permanent magnet motor', *IEEE Trans. Ind. Electron.*, 1988, **35**, (4), pp. 537–541
[25] Chapra, S.C., Canale, R.P.: '*Numerical methods for engineers*' (McGraw-Hill, McGraw-Hill Education, New York, NY, USA, 2015, 7th Edn.)
[26] Kukrer, O.: 'Discrete-time current control of voltage-fed three-phase PWM inverters', *IEEE Trans. Power Electron.*, 1996, **11**, (2), pp. 260–269

7 Appendix

A closed-loop characteristic equation of the DOB in (20) is expressed as (see (21)) , where

$$
\begin{aligned}
p_0 &= l_1\left(l_1 + \frac{R_nT_s}{L_{dn}} + \frac{R_nT_s}{L_{qn}} - 2\right) \\
&\quad + l_2\left(\frac{T_s^2}{L_{dn}L_{qn}}l_2 + 2\frac{R_nT_s^2}{L_{dn}L_{qn}} - \frac{T_s}{L_{dn}} - \frac{T_s}{L_{qn}}\right) \\
&\quad + l_1l_2\left(\frac{T_s}{L_{dn}} + \frac{T_s}{L_{qn}}\right) + \left(\frac{(R_nT_s)^2}{L_{dn}L_{qn}} - \frac{R_nT_s}{L_{dn}} - \frac{R_nT_s}{L_{qn}} + 1\right) \\
p_1 &= l_1\left(-2l_1 - 2\frac{R_nT_s}{L_{dn}} - 2\frac{R_nT_s}{L_{qn}} + 6\right) \\
&\quad + l_2\left(2\frac{T_s}{L_{dn}} + 2\frac{T_s}{L_{qn}} - 2\frac{R_nT_s^2}{L_{dn}L_{qn}}\right) - l_1l_2\left(\frac{T_s}{L_{dn}} + \frac{T_s}{L_{qn}}\right) \\
&\quad + \left(3\frac{R_nT_s}{L_{dn}} + 3\frac{R_nT_s}{L_{qn}} - 2\frac{(R_nT_s)^2}{L_{dn}L_{qn}} - 4\right) \\
p_2 &= l_1\left(l_1 + \frac{R_nT_s}{L_{dn}} + \frac{R_nT_s}{L_{qn}} - 6\right) + l_2\left(-\frac{T_s}{L_{dn}} - \frac{T_s}{L_{qn}}\right) \\
&\quad - \left(3\frac{R_nT_s}{L_{dn}} + 3\frac{R_nT_s}{L_{qn}} - \frac{(R_nT_s)^2}{L_{dn}L_{qn}} - 6\right) \\
p_3 &= 2l_1 + \frac{R_nT_s}{L_{dn}} + \frac{R_nT_s}{L_{qn}} - 4 \\
p_4 &= 1.
\end{aligned}
$$

$$
\begin{aligned}
\det\left[z\boldsymbol{I} - (\boldsymbol{\Phi} - \boldsymbol{LH})\right] &= \det\left[z\boldsymbol{I} - \left(\begin{bmatrix}\boldsymbol{A}_n(k) & -\boldsymbol{B}_n \\ 0 & \boldsymbol{I}\end{bmatrix} - \begin{bmatrix}l_1\boldsymbol{I} & 0 \\ 0 & l_2\boldsymbol{I}\end{bmatrix}\begin{bmatrix}\boldsymbol{I} & 0\end{bmatrix}\right)\right] \\
&= p_4z^4 + p_3z^3 + p_2z^2 + p_1z + p_0 \\
&= 0
\end{aligned} \tag{21}
$$